*metals*

MDPI

*Article*

# Fabrication and Characterization of In Situ Ti-6Al-4V/TiB Composites by the Hot-Pressing Method using Recycled Metal Chips

**Yutao Zhai [1], Ajit Pal Singh [1], Leandro Bolzoni [1], Yingdong Qu [2], Yiming Li [3] and Fei Yang [1,*]**

[1] Waikato Centre of Advanced Materials and Manufacturing, School of Engineering, The University of Waikato, Hamilton 3240, New Zealand
[2] School of Materials Science and Engineering, Shenyang University of Technology, Shenyang 110870, China
[3] Analytical and Testing Center, School of Materials Science and Engineering, Inner Mongolia University of Science and Technology, Baotou 014010, China
* Correspondence: fei.yang@waikato.ac.nz

**Abstract:** In this study, a Ti-6Al-4V matrix composite reinforced with in situ synthesized TiB whiskers has been successfully produced from wasted chips by a cost-effective powder metallurgy route combining rapid heating and hot pressing. The effect of boron powder addition (1 vol.%, 3 vol.%, 5 vol.%, and 7 vol.%) on phase constituents, microstructures, and mechanical properties of the fabricated composites was investigated. Additionally, the effect of two different post-heat treatments on the 3 vol.% boron-containing composites was also explored. The results show that the ultimate tensile strength (UTS) and yield strength (YS) of the composite first increase when the content of boron is less than 3 vol.%, and then start to decrease with the further increase of boron content. The TiB reinforcement layers change from discontinuous to quasi-continuous and then to continuous with increasing boron content, which is attributed to a higher fraction of agglomerated TiB reinforcement phases. The composites with 1 vol.% (UTS of 1085 MPa, strain to fracture of 5.83%) and 3 vol.% (UTS of 1127 MPa, strain to fracture of 3.98%) boron powder addition show optimized tensile properties. The mechanical properties of 3 vol.% boron-containing composites are not significantly improved after heat treatment. Our experimental results demonstrate the feasibility of fabricating low-cost, high-performance titanium alloy matrix composites from Ti-6Al-4V machining chips. It can serve as a promising and cost-effective method to directly utilize Ti-6Al-4V chips to fabricate strong and ductile Ti-6Al-4V composites for niche applications.

**Keywords:** titanium chips recycling; titanium matrix composites; TiB whiskers; microstructure evolution; hot pressing consolidation; mechanical properties; in situ composite



**Citation:** Zhai, Y.; Singh, A.P.; Bolzoni, L.; Qu, Y.; Li, Y.; Yang, F. Fabrication and Characterization of In Situ Ti-6Al-4V/TiB Composites by the Hot-Pressing Method using Recycled Metal Chips. *Metals* **2022**, *12*, 2038. https://doi.org/10.3390/met12122038

Academic Editor: Antonio Mateo

Received: 26 October 2022
Accepted: 23 November 2022
Published: 27 November 2022



## 1. Introduction

In recent years, titanium matrix composites (TMCs) have attracted a lot of attention due to their excellent mechanical properties and the variety of materials with a wide range of physical and chemical properties [1,2]. Out of various well-established titanium matrix composites, Ti-6Al-4V matrix composites show a higher potential demand in aerospace, military, and biomedical fields due to their high specific strength, high heat resistance, and corrosion resistance [3–5]. Compared with TMCs fabricated using ex situ processes, the in situ synthesis process can overcome the contamination and wettability issues between the reinforcement phase and the metal matrix, resulting in better interfacial bonding strength [6,7]. Currently, many in situ composite techniques, such as casting, mechanical alloying (MA), powder metallurgy (PM), and selective laser melting (SLM), have been widely used to fabricate TMCs [8–10].

Ingot/wrought titanium alloy parts are very expensive because of their high raw material costs, high energy consumption during manufacturing processing, and high buy-to-fly ratio (80% of the starting material becomes scrap during processing) [11–14]. Most of

the established recycling methods are melt-based (i.e., remelting recycling) [15–18], which require high energy consumption and are not very environmentally friendly. The solid-state recycling route is gaining more attention each passing day as an attractive strategy to develop low-cost and high-performance titanium alloys from wasted chips [13,14,19–21].

Various researchers had consolidated the commercially pure (CP) titanium and Ti-6Al-4V machining chips into full-dense parts using equal channel angular pressing (ECAP) at relatively low temperatures (400–600 °C) [12,13,22]. The consolidated CP-titanium had provided YS up to 650 MPa and strain to fracture of 16%, whereas in the case of the Ti-6Al-4V alloy, YS as high as 900 MPa along with ductility of 11% was achieved. Recently, Yang et al. [19] had consolidated as-received Ti-6Al-4AV chips into near-fully dense Ti-6Al-4V billets by hot pressing (HP), which have a YS of 928–998 MPa, a UTS of 1076–1143 MPa, and a ductility between 6.92 and 7.80%.

Several studies have been reported in the literature that discuss the reinforcement of Ti-6Al-4V matrix with boron and how the resulting TiB phase (TiBw) provides the perfect combination of mechanical properties in titanium matrix composites (TMCs) [23–26]. It is a well-known fact that boron is essentially insoluble in the titanium and titanium alloy matrix, and the TiB reinforcement phase formed by adding boron elements is formed through an in situ reaction and exists in the whisker shape [23,27]. There is no study reported in the literature that consolidates Ti-6Al-4V chips using severe plastic deformation (SPD) techniques to fabricate titanium alloy matrix composite. The development of titanium alloy matrix composites using direct hot pressing of titanium alloy chips could potentially be suitable for a variety of non-critical potential applications perhaps in the civil construction industry as a structural material, the development of titanium-based metal matrix composites using direct hot pressing of the Ti alloy machining chips can extend the usage in more niche applications. In this research, we will explore the hot processing approach to produce in situ synthesized Ti-6Al-4V/TiB composite materials directly from the as-received Ti-6-Al-4V machining chips and a variable amount of boron powder addition. Additionally, the effect of various post-heat treatments on the microstructure and mechanical properties of 3 vol.% boron-containing composites will be investigated in depth. The aim of this work was to explore the feasibility of fabricating titanium alloy matrix composites from Ti-6Al-4V machining chips and establish a relationship among the boron addition, heat treatment process, and mechanical properties of the composites.

## 2. Experimental Process

Ti-6Al-4V chips (length $\approx$ 15 mm) were collected at the Commercial Machining Operations Centre for Additive Manufacturing, RMIT University, Melbourne, Australia. The morphology of as-received chips and their microstructure are included in Figure 1. The bright phase in Figure 1b is $\alpha$ and the dark phase is $\beta$. It is clear that individual chips are composed of a coarse Widmanstätten structure [28] containing 200–250 μm sized grains and individual laths ($\alpha$ phases) ranging between 150 and 200 μm in length and from 5 to 8 μm in thickness. The thicknesses (122–183 μm) of the Ti-6Al-4V chips and the amorphous boron powder from Sigma Aldrich, St. Louis, MO, USA (assay $\geq$ 95%, particle size $\leq$ 1 μm) are shown in Figure 1c and d, respectively. The oxygen content of the chips was measured using the LECO method, and the determined value was 0.15 wt%.

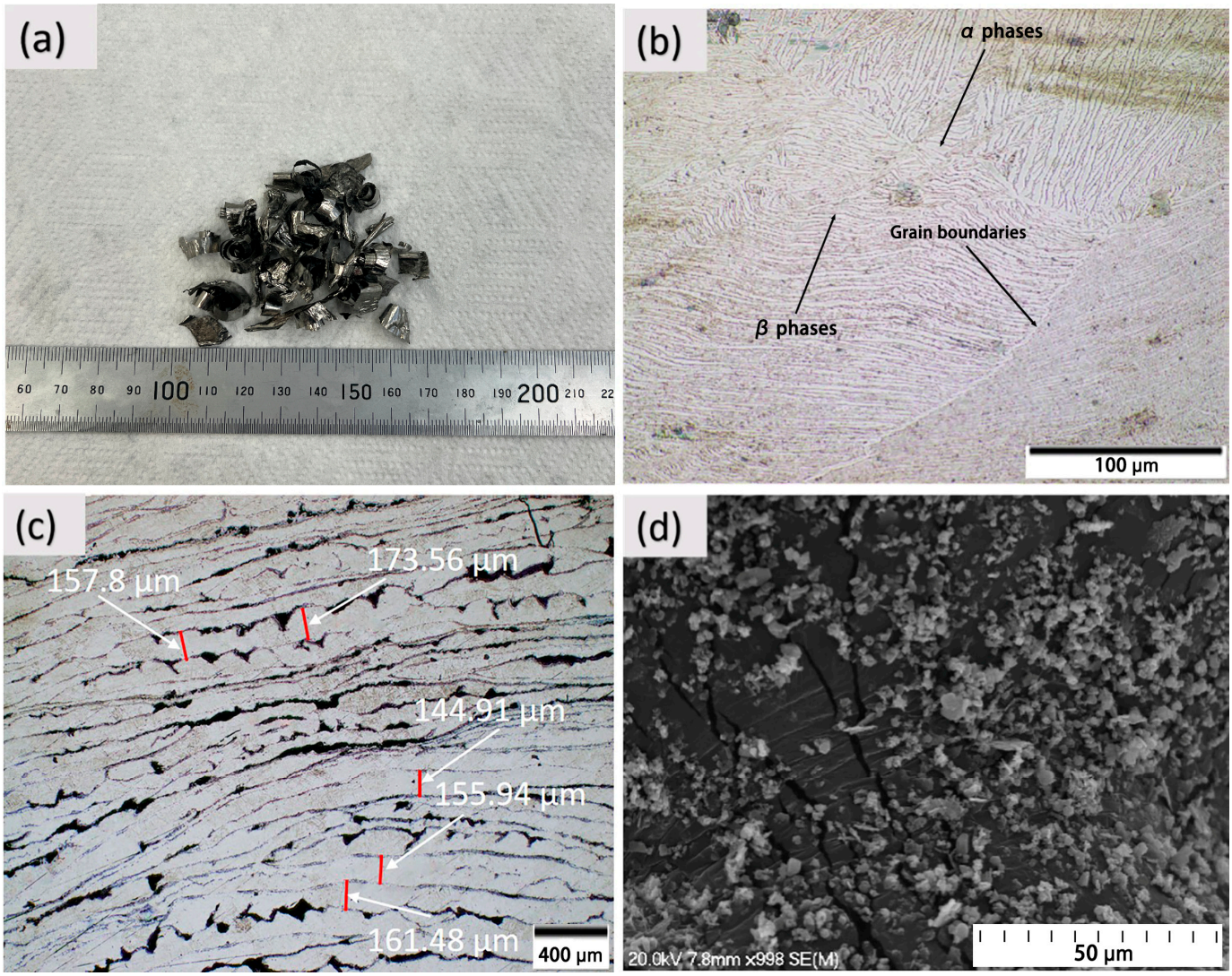


**Figure 1.** (**a**) As-received Ti-6Al-4V chips; (**b**) initial microstructures of as-received chips; (**c**) thickness of Ti-6Al-4V chips before hot pressing; and (**d**) amorphous boron powder.

To remove the residual coolant and dust, the chips were rinsed in hot water with a dishwashing liquid, followed by ultrasonic cleaning in 99.5% ethanol for 1 h. Then, the Ti-6Al-4V chips were crushed into small chips. The well-cleaned chips and x vol.% (x = 1, 3, 5, and 7) of boron powder were mixed in a V-type mixer (Jiangyin Rongde Machinery, Jiangyin, China) at a speed of 60 rpm, and the mixing time was 120 min. After that, the well mixed chip mixture was warmly compacted into green compacts (56 mm in diameter and 28 mm in height) at 250 °C prior to hot processing. The compact was subsequently heated up to 1250 °C using an induction furnace (Inductotherm Ltd., Seaford, Australia) and then hot pressed into a cylinder-shape billet (58 mm in diameter and 18 mm in height) using a 100 ton hydraulic press (Inductotherm Ltd., Seaford, Australia). The applied pressure was 400 MPa, and the hot-pressing time was 90 s. The whole hot-pressing process is under the protection of Ar gas ($O_2$ < 200 ppm). Thus, the change in oxygen content of the composite material after hot pressing is negligible. For details on the change in oxygen content, refer to reference [14]. Figures 2 and 3 show a schematic illustration of the hot-pressing process and the appearance of green compacts and hot-pressed billets. In-depth experimental details regarding the hot-pressing procedures can be found in the references [29,30].

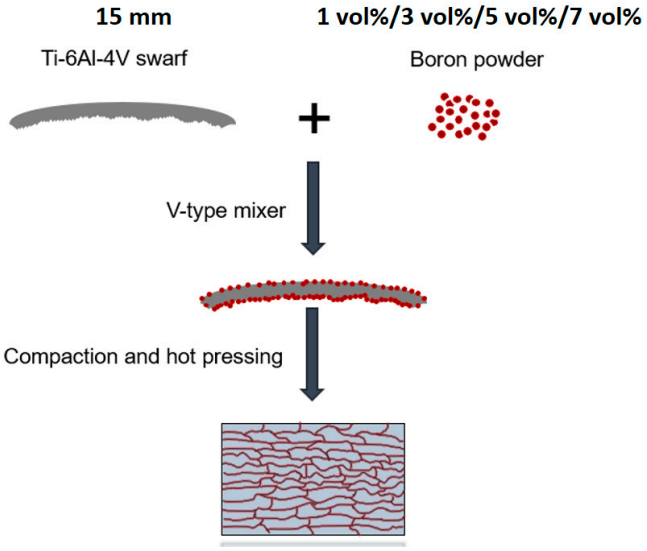


**Figure 2.** Schematic illustration of the powder mixing and hot-pressing process.

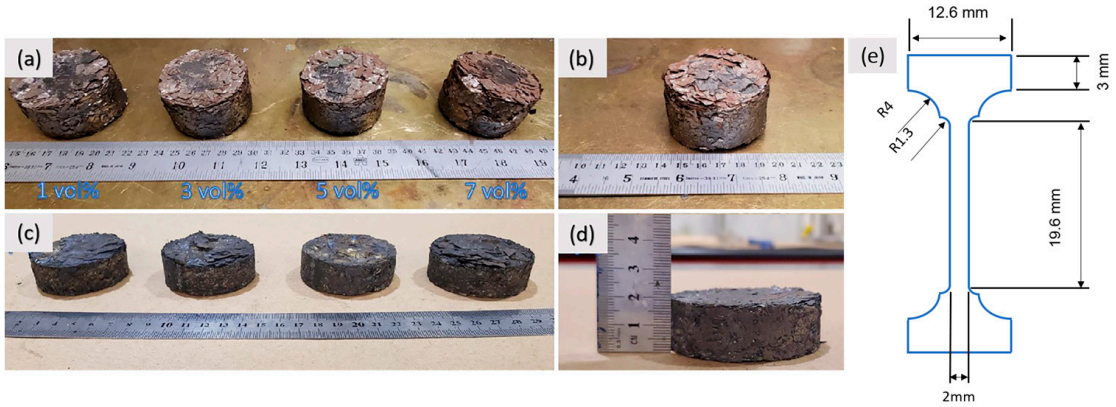


**Figure 3.** Appearances of chips Ti-6Al-4V matrix composite samples (**a**) 250 °C warm-compacted green compacts; (**b**) a single compact after warm compaction; (**c**) hot-pressed billets; (**d**) a single hot-pressed billet; and (**e**) a dog-bone-shaped specimen.

The constituent phases were characterized using an X-ray diffractometer (XRD) (Philips X'Pert system, Malvern, UK). The diffractometer using CuK$\alpha$ (1.5406 Å) radiation uses an angular scanning interval of 2$\theta$ from 30 to 100°. The step size was 0.013°, with a voltage of 45 KV and a current of 40 mA. The microstructures were examined using an optical microscope (Olympus BX60, Olympus Optical Co. Ltd., Tokyo, Japan) and scanning electron microscopy (SEM, Hitachi-S4000, Hitachi, Tokyo, Japan). The phase ratios in Tables 3 and 4 were measured by Image-Pro Plus software (version 6.0, Media Cybernetics, Rockville, MD, USA). The samples for microstructure observations were prepared using standard procedures of grounding (SiC paper), polishing (silica gel), and etching using a modified Kroll's reagent [14,31] consisting of 10 vol.% HF, 20 vol.% $HNO_3$, and 70 vol.% $H_2O$. The dog-bone-shaped tensile specimens (Figure 3e) were prepared from the hot-pressed composites and conducted on an Instron universal testing machine (INSTRON 4204, Instron Pty Ltd., Melbourne, Australia) at a strain rate of $10^{-4}$ $s^{-1}$, and the fracture surfaces of the tensile sample were characterized by SEM. Heat treatment is performed for the sample of Ti-6Al-4V with 3 vol.% boron powder in the muffle furnace, and the conditions of the heat treatment are based on previous works and shown in Table 2. The densities and Vickers hardness of the composites were measured using Archimedes' principle and a Future-Tech FM-700 (2000 g/10 s) microhardness tester, respectively.

For convenience in the following sections, the hot-pressed composites produced from the mixture of Ti-6Al-4V chips and x vol.% of boron addition (x = 1, 3, 5, and 7) will be denoted by the label Chips-Ti64-xTiB (Table 1). Similarly, composites containing 3 vol.% boron (Chips-Ti64-3TiB) subjected to heat treatment: hold at 855 °C for 1 h, water quenching plus aging at 550 °C for 6 h followed by air cooling and will be donated under the label Chips-STA-855. The same starting material underwent a second heat treatment: hold at 955 °C for 1 h, water quenching plus aging at 550 °C for 6 h, followed by air cooling and will be represented by the label Chips-STA-955 (Table 2).

**Table 1.** Detailed information of Ti-6Al-4V chips with x vol.% of boron addition (x = 1, 3, 5, and 7).

| Sample Label | Starting Materials | Density (g/cm$^3$) |
|---|---|---|
| Chips-Ti64-1TiB | chips Ti-6Al-4V + 1 vol.% boron | 4.423 |
| Chips-Ti64-3TiB | chips Ti-6Al-4V + 3 vol.% boron | 4.395 |
| Chips-Ti64-5TiB | chips Ti-6Al-4V + 5 vol.% boron | 4.390 |
| Chips-Ti64-7TiB | chips Ti-6Al-4V + 7 vol.% boron | 4.351 |

**Table 2.** The details of two heat treatments performed on Chips-Ti64-3TiB composite material.

| Heat Treatment Type | Solution Treatment and Aging |
|---|---|
| STA-855 | 855 °C for 1 h water quenching + 550 °C 6 h air cooling |
| STA-955 | 955 °C for 1 h water quenching + 550 °C 6 h air cooling |

## 3. Result and Discussion

### *3.1. Microstructural Analysis*

Figure 4 shows the XRD patterns of the hot-pressed composite material produced from Ti-6Al-4V chips with x vol.% (x = 1, 3, 5, and 7) of boron powder addition. The peaks of α phase, β phase, and TiB appeared in all different compositions. Only one reinforcement in situ phase (TiB) is identified in each composite, whose intensity in XRD patterns increases with increasing the volume fraction of boron addition.

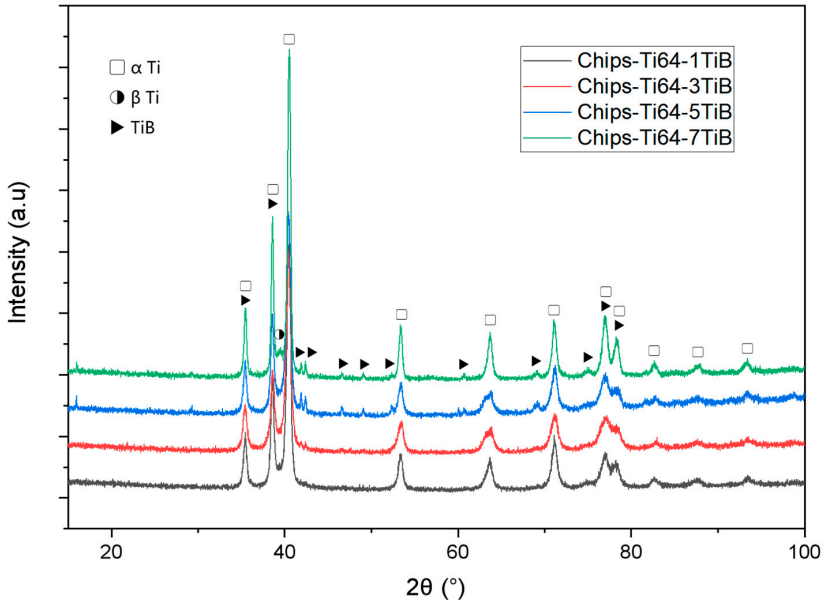


**Figure 4.** XRD patterns of 1250 °C hot-pressed Ti-6Al-4V composites with x vol.% Boron (x = 1, 3, 5, and 7).

The TiB whiskers are in situ synthesized via the following three reactions (1–3):

$$Ti + B = TiB \quad (1)$$

$$Ti + 2B = TiB_2 \quad (2)$$

$$Ti + TiB_2 = TiB \quad (3)$$

Further detail about the reactions and chemistry between titanium and boron powder can be found in [24,32]. Generally, if there is an excess of titanium, thermodynamically unstable $TiB_2$ completely reacts with titanium and forms TiB. In the present study (Figure 4), there is evidence that the reaction (3) took place and was completed under the designed experimental parameters.

Figure 5 shows the optical microstructures of the fabricated composites. It is clear that the Chips-Ti64-5TiB composite has distinct identification of TiB morphology and grain boundary structure at low resolution. Other composites either have an insufficient amount of TiB phase or significant agglomeration when examined using low-magnification microscopes. Due to this reason, the only in-depth microstructural analysis results performed on Ti-6Al-4V with 5 vol.% boron addition composites are included in this segment. Figure 6 shows the schematic of the cross-section of the hot-pressed Chips-Ti64-5TiB composite and nine different locations from where the optical microstructures were captured (Figure 6a). It can be clearly seen that the interval of TiB is approximately the same as the thickness of Ti-6Al-4V chips (122–183 µm). The upper and lower surfaces of the composite contact the die and the punch, causing a large heat dissipation, so the unclosed prior-chip boundaries can be seen at the top and bottom of the billet. The sample observed and tested in the following sections is cut from the central part of the billets.

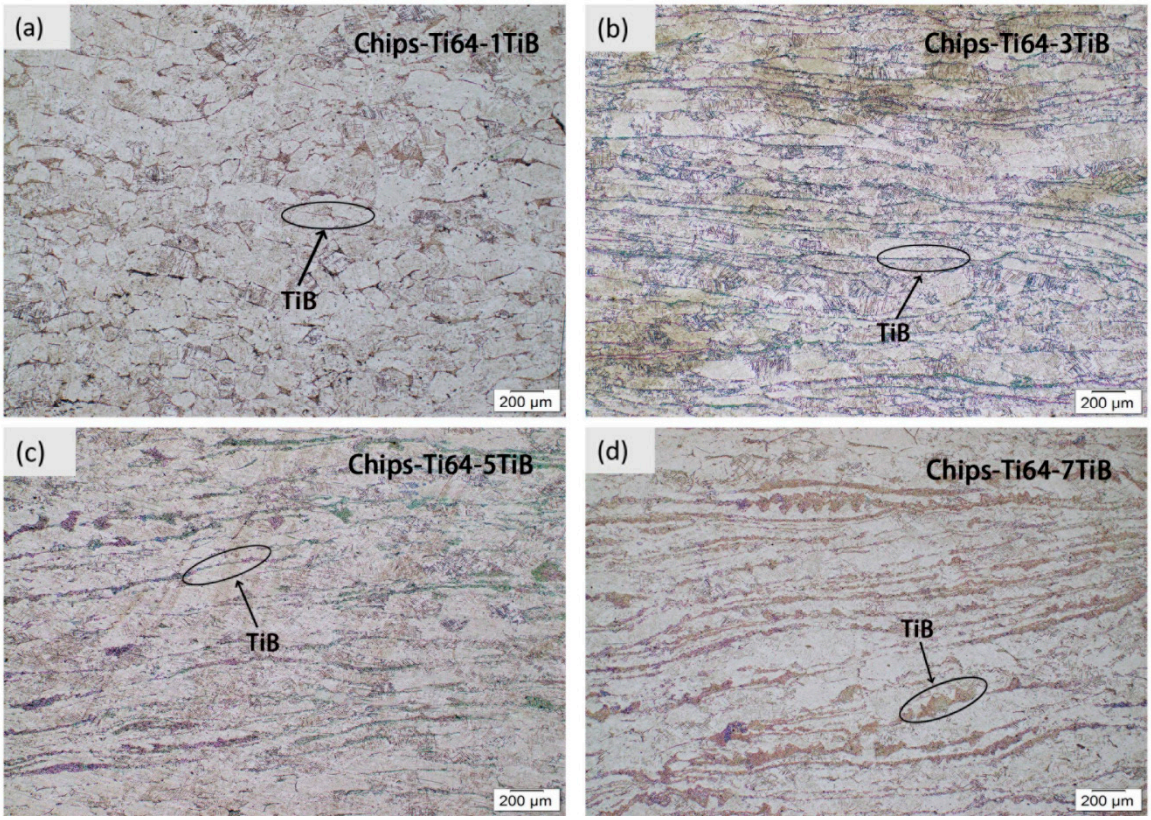


**Figure 5.** The optical microstructures of 1250 °C hot-pressed Chips-Ti64-xTiB composites: (**a**) Chips-Ti64-1TiB; (**b**) Chips-Ti64-3TiB; (**c**) Chips-Ti64-5TiB; and (**d**) Chips-Ti64-7TiB.

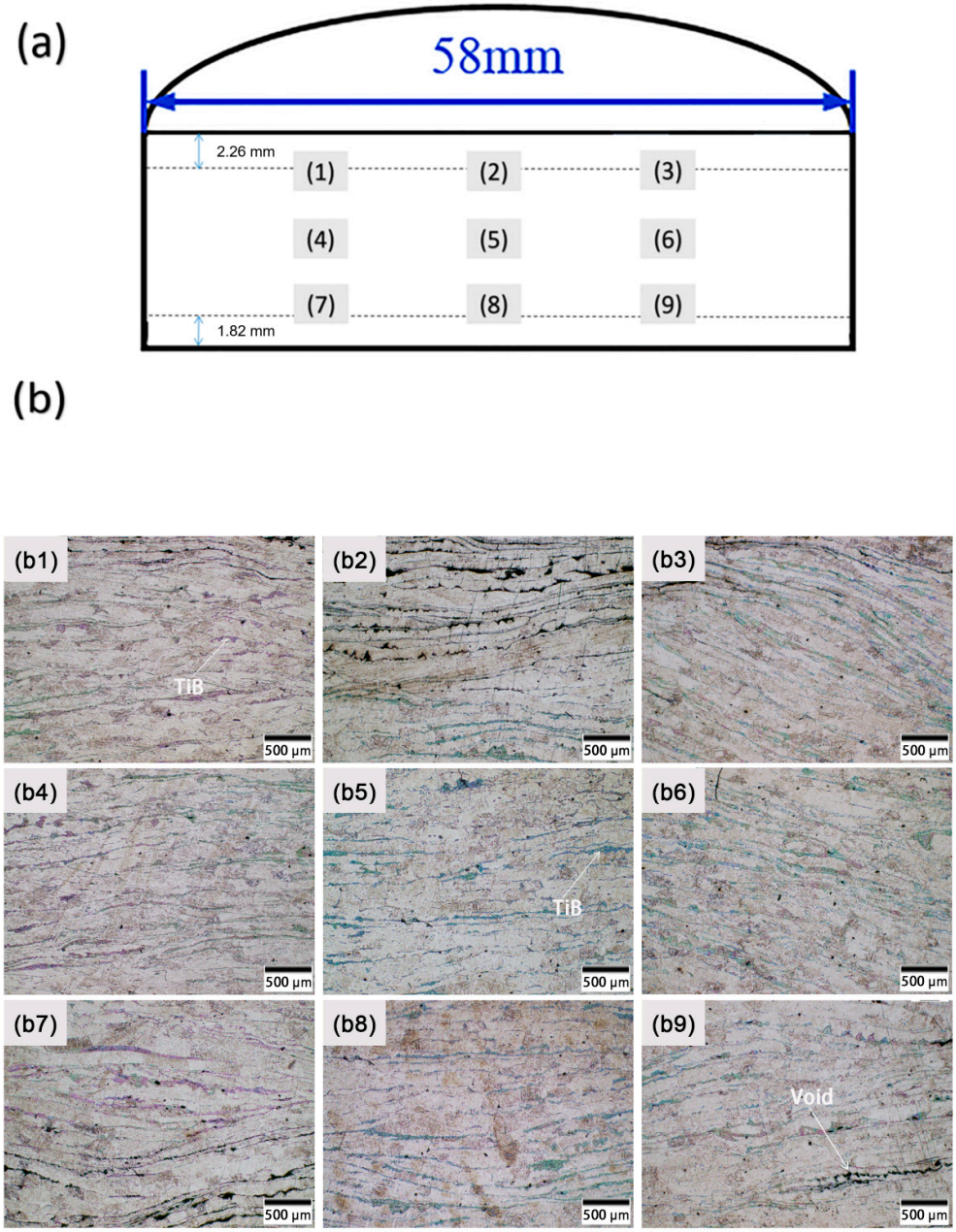


**Figure 6.** (**a**) Schematic drawing of the cross section of the Chips-Ti64-5TiB showing the locations where the microstructures of the material were examined; and (**b**) the optical microstructures of the Chips-Ti64-5TiB composite at nine different points ((**b1**) is the position of 1 in (**a**), (**b2**) is the position of 2 in (**a**), and so on with (**b3**–**b9**).

Figure 7 shows SEM images of Chips-Ti64-xTiB composites. From Figure 7e, the morphology of the TiB reinforcement phase is a short rod (whiskers) shape, and the microstructure of the matrix phase did not change with the increase of the TiB reinforcement. It is composed of the lamellar α phase (the width is 1.5–2 μm and the length is 3–6 μm, as shown in Figure 7f) and the β phase. Figure 7a shows that the size of the grain is roughly the same as the thickness of individual chips, thus it can be inferred that TiB whiskers are located at the prior-chip boundaries [33]. There are basically no agglomerated TiB whiskers observed in Chips-Ti64-1TiB (Figure 7a) and Chips-Ti64-3TiB (Figure 7b). However, TiB clusters are visible in the other two samples, and these become more apparent with increasing volume fractions of boron powder. Some voids were observed in Chips-Ti64-7TiB (Figure 7d), which may be caused by the incomplete reaction due to the uneven

distribution and excessive boron powder during the short hot-pressing process. Furthermore, as the amount of boron powder increases, the morphology of the TiB reinforcement phases changes from discontinuous TiB reinforcement layers (Chips-Ti64-1TiB) → quasi-continuous TiB reinforcement layers (Chips-Ti64-3TiB) → continuous TiB reinforcement layers (Chips-Ti64-5TiB and Chips-Ti64-7TiB). The variation of TiB reinforcement layers and strengthening mechanisms are discussed in Section 3.3.

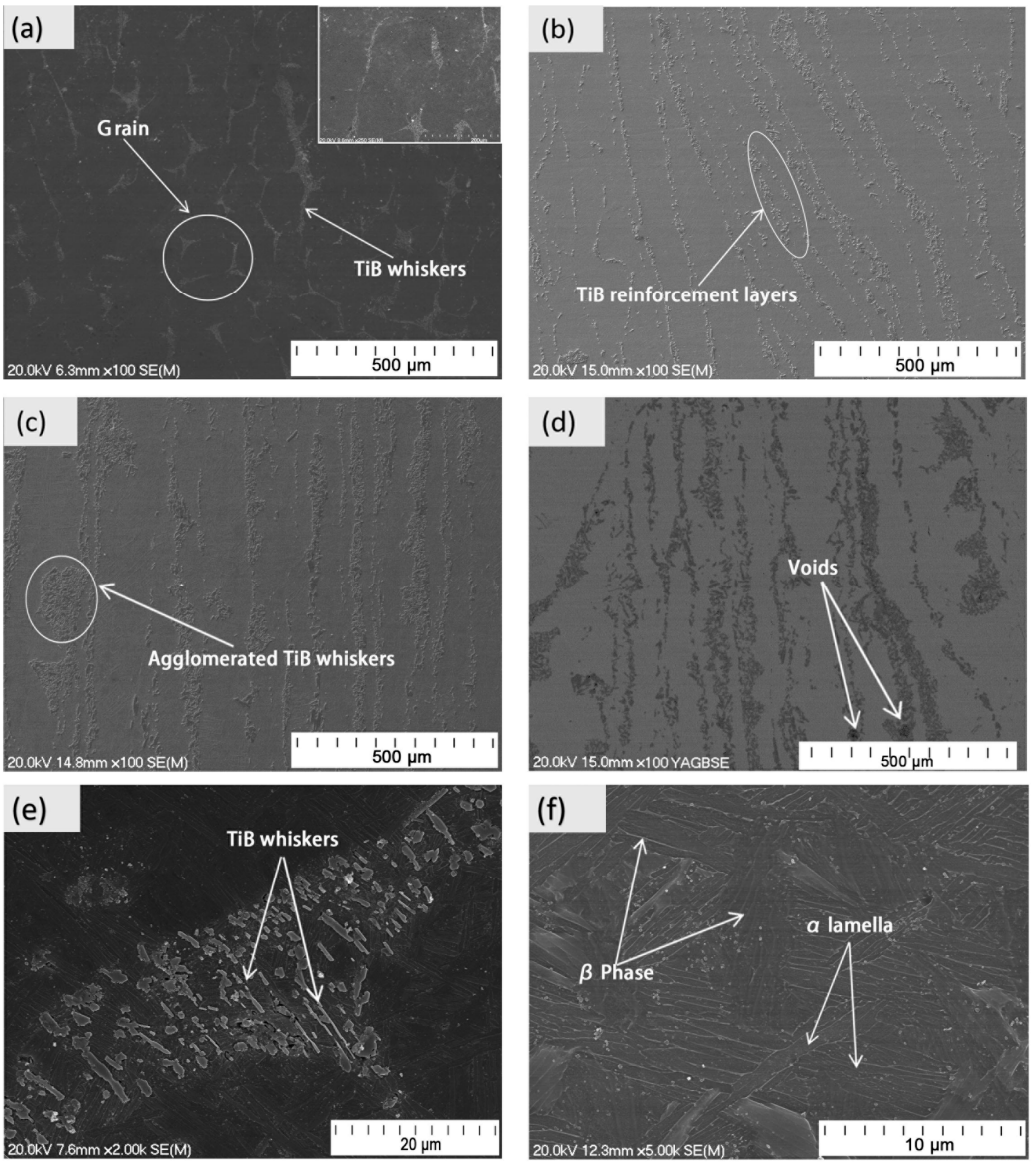


**Figure 7.** SEM images of Chips-Ti64-xTiB composites: (**a**) Chips-Ti64-1TiB; (**b**) Chips-Ti64-3TiB; (**c**) Chips-Ti64-5TiB; (**d**) Chips-Ti64-7TiB; (**e**) TiB reinforcement from Chips-Ti64-1TiB; and (**f**) matrix phase (Ti-6Al-4V) from Chips-Ti-64-3TiB.

Table 3 lists the measured proportions and aspect ratios of TiBws in the Chips-Ti64-xTiB composites. It can be seen from the table that the content of TiBws is close to the nominal composition, and the aspect ratio of TiBws is less than six. TiBws generally grow at a higher growth rate in the longitudinal direction than in the transverse direction [7,34]. In our case, the aspect ratio is relatively small due to the short heating time, fast cooling rate, and insufficient element diffusion time during hot pressing [34–36]. TiBws with a high aspect ratio can effectively improve the strengthening efficiency, but when the aspect ratio is less than 10, the strengthening effect of aspect ratio on the composites is negligible [34,37].

Therefore, in current research, the main factor affecting the mechanical properties is the proportion and distribution of TiBw.

**Table 3.** Aspect ratios and proportion of the TiB whiskers of the TiBw/Ti-6Al-4V composite with different boron additions.

| Composites | Aspect Ratio | TiB Proportion (%) |
|---|---|---|
| Chips-Ti64-1TiB | 2–6 | 1.18 ± 0.04 |
| Chips-Ti64-3TiB | 2–3 | 3.21 ± 0.06 |
| Chips-Ti64-5TiB | 1–3 | 4.78 ± 0.07 |
| Chips-Ti64-7TiB | 1–3 | 6.65 ± 0.15 |

Figure 8 exhibits the microstructures of Chips-Ti64-3TiB heat treated at the conditions of STA-855 and STA-955. Because the martensite transformation temperature of Ti-6Al-4V is around 900 °C, no martensite structure is observed in the Chips-Ti64-3TiB composites after water quenching from 855 °C [38]. Instead, a small proportion of residual β phases remains in the composite after quenching (Figure 8a). The primary α phase present in the composite has a width between 1 and 2.5 μm and a length between 10 and 16 μm (Figure 8a). After aging at 550 °C for 6 h, the size of primary α phase remain unchanged, and the precipitate α phase (in nano size) was observed in transformed β phase (Figure 8c). Chips-Ti64-3TiB composite quenched from 955 °C had martensitic (α′) phase along with primary α phase, with dimensions 1.5–3 μm in width, 6–8 μm in length, 1.5–3 μm in width, and 6–8 μm in length, respectively (Figure 8d). After aging, the aged state consists of decomposed martensite (α′) in the form of an acicular secondary α phase (width of 0.3–0.5 μm and length of 1–5 μm, Figure 8f) + β phase.

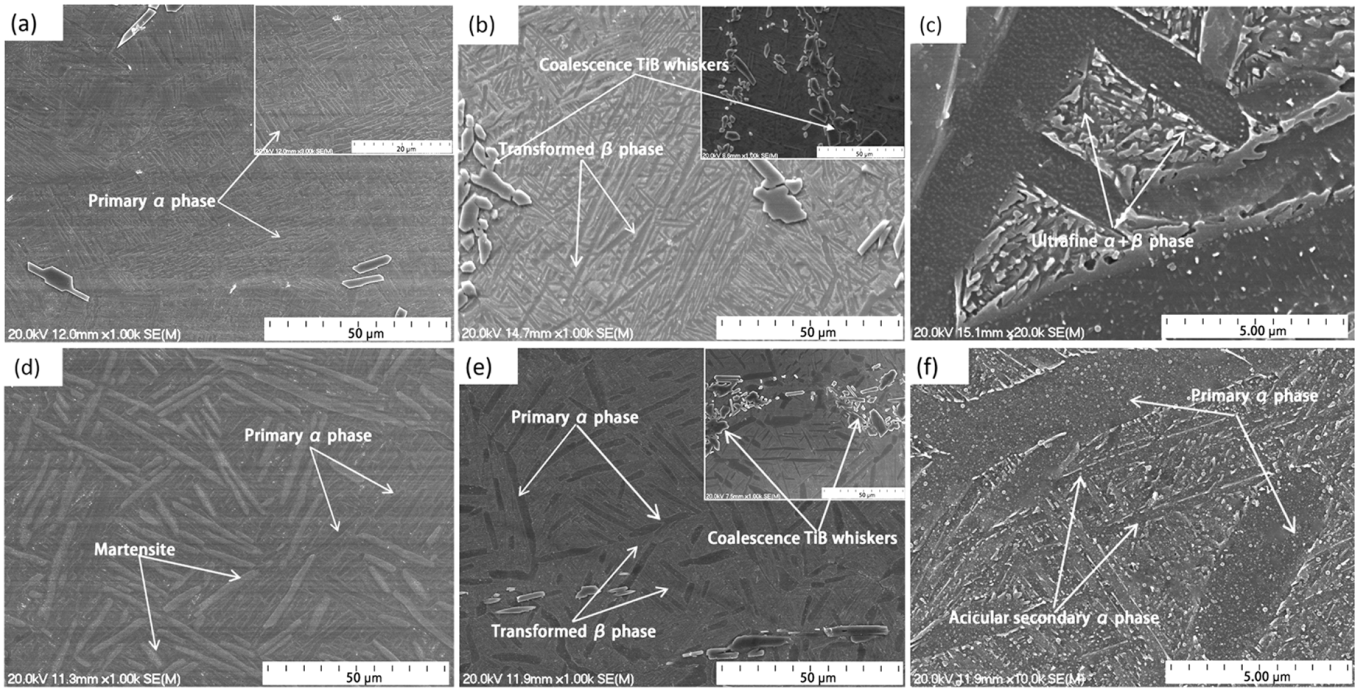


**Figure 8.** SEM images of Chips-Ti64-3TiB composites after heat treatment: (**a**,**d**) 855 °C/1 h and 955 °C/1 h + water quenching; (**b**,**e**) aged at 550 °C/6 h + air cooling; and (**c**,**f**) high magnification images corresponding to (**b**) and (**e**), respectively.

Table 4 shows the phase proportion of Chips-Ti64-3TiB after different heat treatments. Chips-STA-855 shows a higher primary α phase content (76%, measured by Image-Pro Plus) than Chips-STA-955 (28%), and this is attributed to a larger amount of alpha phase existing under a relatively low heat treatment temperature that is below the beta transus temperature.

**Table 4.** Phase proportion of Chips-STA-855 and Chips-STA-955 composites.

| Composites | Phase Proportion (%) | |
|---|---|---|
| | Primary α Phase | Transformed β Phase |
| Chips-STA-855 | 76 ± 1.33 | 24 ± 0.67 |
| Chips-STA-955 | 28 ± 1.33 | 72 ± 1.66 |

TiB whiskers in TMCs are very stable, even when heat-treated at high temperatures [39,40]. However, the TiB whiskers are significantly coarsened in this experiment, changing from a whisker shape to an irregular shape (Figure 8b,e). This is because TiB whiskers will grow along the [100] direction during the heat treatment, forming a (100) stacking plane via the diffusion of boron atoms at high temperature (above 850 °C), resulting in the coalescence between adjacent TiBws [41], which is followed by the Ostwald ripening principle [42,43]. The coalescence of TiBws was observed in the samples Chips-STA-855 and Chips-STA-955, but the difference is not distinct. This is because the difference in the heat treatment temperatures for those two samples is only about 100 °C, and its effect on the TiBws coalescing is insignificant [44,45].

### *3.2. Tensile Properties and Fracture Analysis*

Figure 9 shows the room temperature stress-strain curves of the fabricated Chips-Ti64-xTiB (x = 1, 3, 5, and 7) composites and Chips-Ti64-3TiB after different heat treatments. It is apparent that as the amount of boron increases, the ductility of the material is decreasing significantly. When the boron addition is more than 5 vol.%, the fabricated composites become very brittle, and there is no evidence showing plastic deformation happens. This is mainly attributed to the fact that the TiB reinforcement has become seriously agglomerated (Figure 7c,d). The strength of the Chips-Ti64-3TiB has increased after STA-855 heat treatment, which may be attributed to the refinement of the transformed β phase (Figure 8c) decomposed from martensite (α′) and the release of residual stress [14,19,41]. However, after heat treatment with STA-855, the ductility of the composite has decreased, which is different from the results observed by Zhao et al. [14]. This is because although a large number of relatively fine secondary α precipitates are produced after STA-855 (Figure 8b,c), and the size and shape of the α phase obtained in this way contribute to the excellent mechanical properties (i.e., the α/β interface hinders the movement of dislocations [14,46]), most studies have shown that the morphology, distribution, and content of the reinforcement phase in the composites are the main factors that dominate the changes in material properties [30,43,44]. Therefore, after STA-855, the synergistic effect of the reinforcing phase and the matrix phase leads to improved strength and a decrease in the ductility of the composites. After heat treatment, the changes in mechanical properties, of STA-955 are similar to STA-855, but the ductility is relatively lower due to less primary α phase content (Table 4).

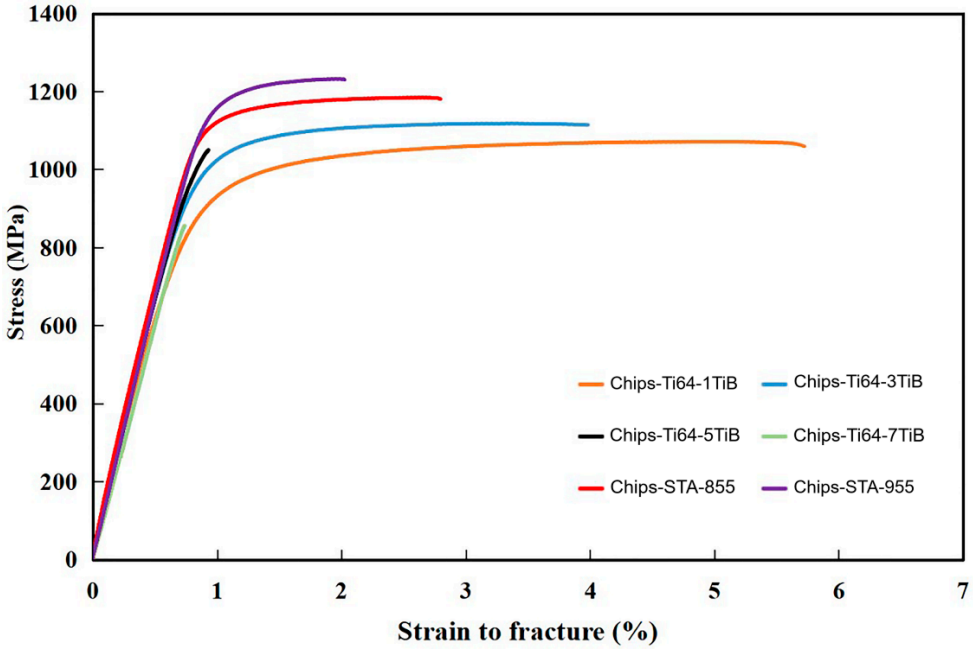


**Figure 9.** Room-temperature stress-strain curves of Chips-Ti64-xTiB composites and Chips-Ti64-3TiB after different heat treatments.

Table 5 displays the tensile properties of the fabricated Chips-Ti64-xTiB composites, and the Chips-Ti64-3TiB after different heat treatments. Chips-Ti64-1TiB has a UTS of 1085 MPa, a YS of 980 MPa, and a strain to fracture of 5.8%. With the content of boron addition increasing to 3 vol.%, the composite's UTS and YS are increased, having a value of 1127 MPa and 1034 MPa, respectively, and the strain to fracture is decreased to 3.98%. Further increasing the boron addition to 5 vol.% and 7 vol.%, the composites have a UTS of 1048 MPa and 855 MPa, respectively. Therefore, it can be concluded that when the small amount of TiB (Chips-Ti64-1TiB and Chips-Ti64-3TiB) is distributed uniformly at the prior chip boundary (Figure 7a,b), it has a positive effect on the strength of the resulting composite material, but the TiB reinforcement decreases the composite's ductility. Chips-STA-855 has a UTS of 1184 MPa, a YS of 1083 MPa, and a strain-to-fracture of 2.78%. Chips-STA-955 has a UTS of 1231 MPa, a YS of 1139 MPa, and a strain to fracture of 2.03%. After STA-855, the UTS and YS of Chips-Ti64-3TiB increased by 5.9% and 4.7%, respectively, and after STA-955, the UTS and YS increased by 10.2% and 10.1%, respectively. The hardness of the composite increases with the addition of boron, and the maximum value is 488.05 HV when the B addition is 7 vol.%. The subsequent STA heat treatment of Chips-Ti64-3TiB leads to an increase in hardness. The increase in hardness can be explained by the decomposition of martensite (STA-955) and the precipitation of the fine $\alpha + \beta$ phase form the transformed $\beta$ phase (STA-855) [26].

Figure 10 shows the SEM fracture morphology of as processed Chips-Ti64-xTiB composites and Chips-Ti64-3TiB after different heat treatments. Features such as a significant amount of cleavage (such as cleavage facets and a tear ridge) and some ductile dimples are quite apparent on the fracture surfaces of Chips-Ti64-1TiB and Chips-Ti64-3TiB (Figure 10a,b). More cleavage facets and almost no ductile dimples were observed on the fracture surface of the composites containing a much higher content of boron addition at Chips-Ti64-5TiB and Chips-Ti64-7TiB (Figure 10c,d), indicating a further reduction in the ductility of the composite. These observations of fracture characteristics are well aligned with the tensile results discussed earlier. Furthermore, aggregates of TiB whiskers and particles can be important crack initiators, and contribute to the poor ductility of the composites. Figure 10e,f show the SEM fracture morphology after heat treatment. The characteristics of brittle fracture can be clearly observed, and more cleavage facets are observed than before heat treatment, especially after STA-955 heat treatment.

**Table 5.** Mechanical properties of the fabricated Chips-Ti64-xTiB composites and Chips-Ti64-3TiB after different heat treatments.

| Composites | Ultimate Tensile Strength (UTS)/MPa | Yield Strength (YS)/MPa | Strain to Fracture % | Hardness (HV) |
|---|---|---|---|---|
| Chips-Ti64-1TiB | 1085 ± 16 | 980 ± 8 | 5.83 ± 0.8 | 334.43 ± 5 |
| Chips-Ti64-3TiB | 1127 ± 13 | 1034 ± 12 | 3.98 ± 0.6 | 389.05 ± 10 |
| Chips-Ti64-5TiB | 1048 ± 18 | - | 0.92 ± 0.08 | 431.70 ± 17 |
| Chips-Ti64-7TiB | 855 ± 20 | - | 0.72 ± 0.1 | 488.05 ± 10 |
| Chips-STA-855 | 1184 ± 11 | 1083 ± 6 | 2.78 ± 0.3 | 420.53 ± 5 |
| Chips-STA-955 | 1231 ± 10 | 1139 ± 4 | 2.03 ± 0.5 | 449.02 ± 14 |

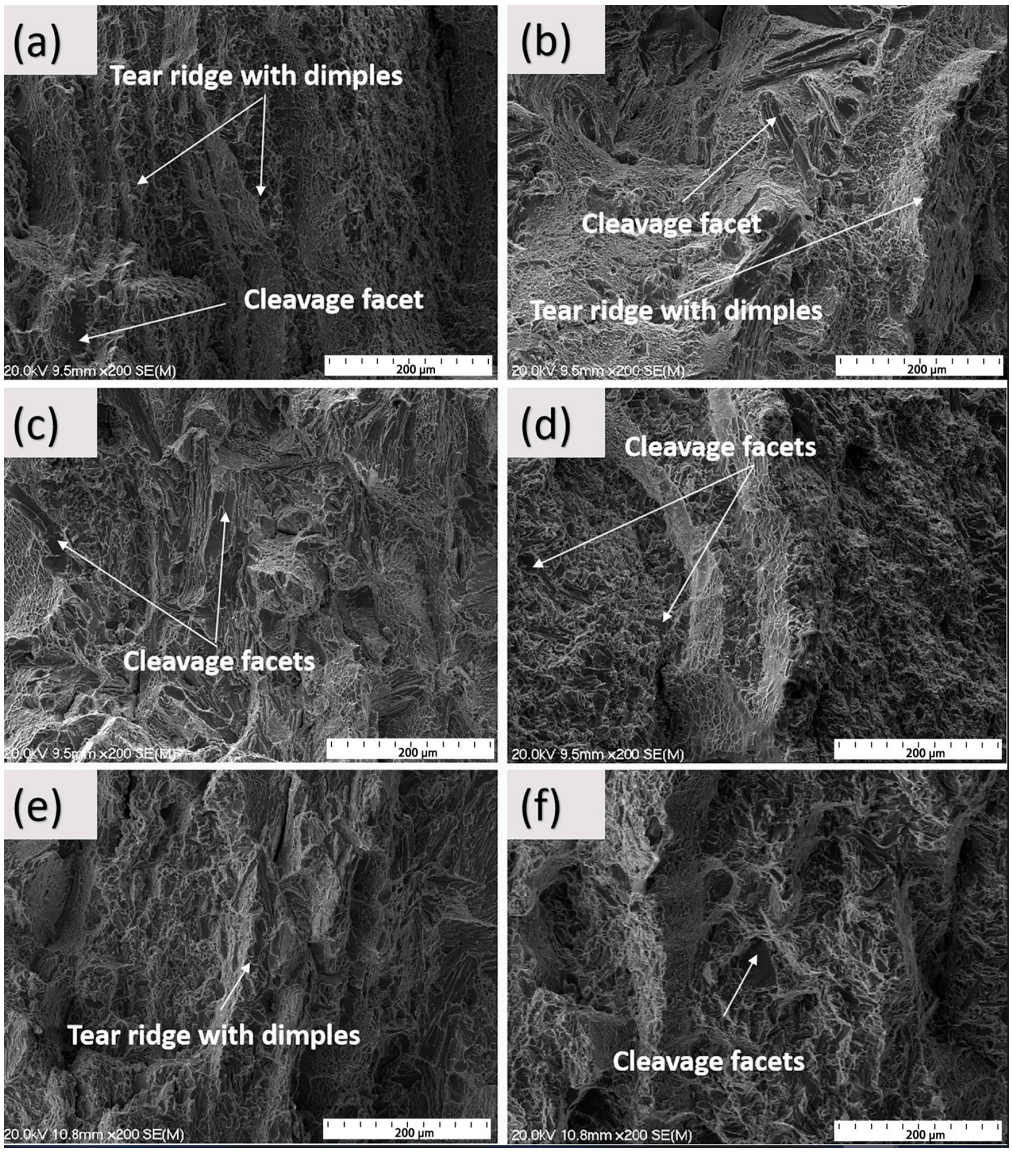


**Figure 10.** SEM fracture morphology of as-processed composites: (**a**) Chips-Ti64-1TiB; (**b**) Chips-Ti64-3TiB; (**c**) Chips-Ti64-5TiB; (**d**) Chips-Ti64-7TiB; (**e**) Chips-STA-855; and (**f**) Chips-STA-955.

SEM images of the longitudinal sections of tensile test specimens cut from different samples are displayed in Figure 11. TiB whiskers fractured in several places were observed, which indicates that a good bonding strength between the TiB whiskers and the Ti-6Al-4V matrix was established after the hot pressing and the TiB whiskers effectively carry a higher load than the matrix phase [6,7]. In addition, the crack propagation near the TiB whiskers also provides evidence for the strengthening effect of reinforced TiB whiskers and strong interfaces. The tortuous routes along the cracks show that the matrix phases fractures when the boron addition is <3 vol.%, and the fracture occurs in the TiB reinforcements when the boron addition is >5 vol.%, which further supports the aggregation of TiB and deteriorates the aggregates properties. (Figure 11c,d).

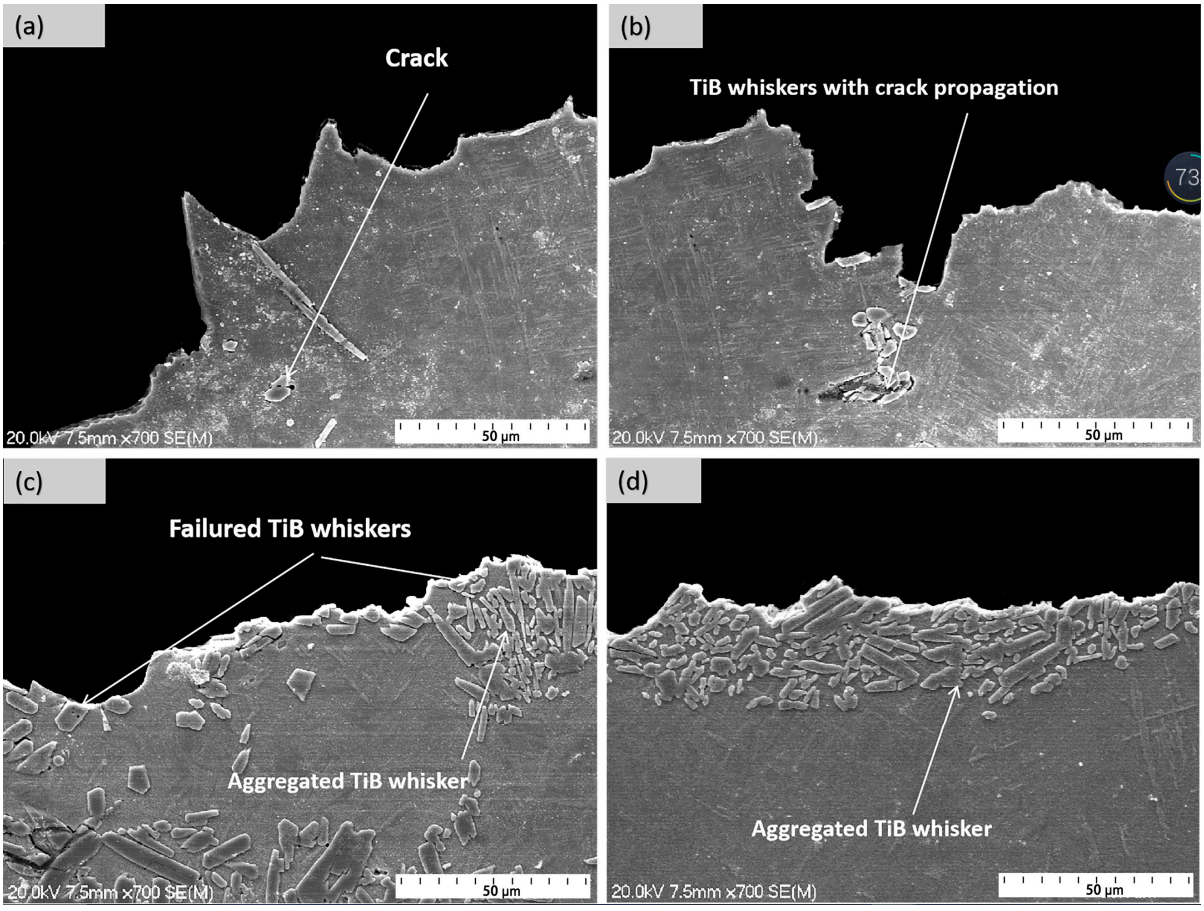


**Figure 11.** SEM images of the longitudinal sections of tensile test samples cut from different samples: (**a**) Chips-Ti64-1TiB; (**b**) Chips-Ti64-3TiB; (**c**) Chips-Ti64-5TiB; and (**d**) Chips-Ti64-7TiB.

Figure 12 shows the comparison of the tensile strength and ductility of Ti-6Al-4V alloys/composites in this study and those of Ti-6Al-4V alloys/composites fabricated by other approaches. It can be clearly seen that the composite material made by Ti-6Al-4V chips not only meets the requirements of industrial applications but also has strength and ductility equal to or greater than those of Ti-6Al-4V alloys/composites made by other methods. Using Ti-6Al-4V chips to fabricate composite materials is more environmentally friendly, and the cost of titanium alloy composite can be greatly reduced, which is beneficial to the wide application of titanium alloy.

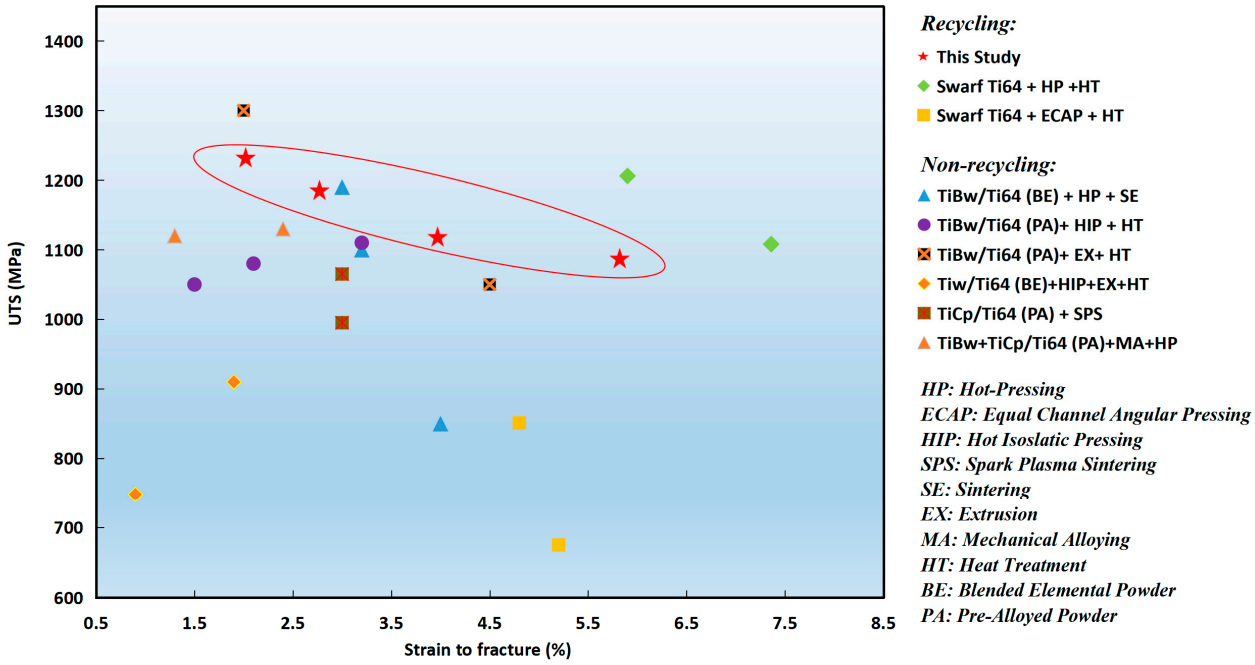


**Figure 12.** Comparison of tensile strength and ductility of Ti-6Al-4V alloys/composites with other approaches and raw materials [8,14,19,35,45,47–50].

### *3.3. Microstructural Evolution and Strengthening Mechanisms*

Table 5 shows that the tensile strength of the composite first increases and then decreases. However, the ductility continues to decrease. This is because the boron powder accumulates on the surface of Ti-6Al-4V chips, resulting in TiB aggregation after hot pressing. Therefore, it can be speculated that the tensile properties of TiB/Ti-6Al-4V composites could be related to the distribution of TiB phases. According to [51], the relationship between the distribution ratio ($D_R$) of boron particles attached to the surface of Ti-6Al-4V chips can be expressed as the following equation:

$$R_D = \frac{mR\rho_{Ti64}}{4Mr\rho_{Boron}} \tag{4}$$

in Equation (4), $\boldsymbol{R}$, $\boldsymbol{\rho_{Ti64}}$, and $\boldsymbol{M}$ are the radius, density, and mass percent of the Ti-6Al-4V particle, respectively, and $\boldsymbol{r}$, $\boldsymbol{\rho_{Boron}}$, and $\boldsymbol{m}$ are those of the boron powder. According to the conclusion of Chao Cai et al. [51], the main influencing factor that affects the $D_R$ is mass percent ($\boldsymbol{M}$ and $\boldsymbol{m}$), due to the large size difference between $\boldsymbol{R}$ and $\boldsymbol{r}$:

$$R_D = \frac{mR\rho_{Ti64}}{4Mr\rho_{Boron}} \tag{5}$$

combining Equations (4) and (5) yields the following equation:

$$R_D = \frac{V_{Boron}R}{4V_{Ti64}r} \tag{6}$$

it can be seen from Equation (6) that as the volume fraction of the boron powder increases ($V_{Boron}$), the distribution ratio ($D_R$) gradually increases. For the sample containing 1 vol.% boron addition, most of the surface area of the mixed Ti-6Al-4V chips is not covered by boron particles, resulting in discontinuous TiB reinforcement layers. As the volume fraction of boron powder increases ($V_{Boron}$), the coverage of boron powder on the surface of Ti-6Al-4V chips gradually increases, resulting in the formation of quasi-continuous (3 vol.%) and continuous (5 vol.% and 7 vol.%) TiB reinforcement layers after hot pressing (see Figure 6). The coalescence of TiBws after heat treatment results in a decrease in the proportion of

free grain boundaries. Therefore, after heat treatment (STA-855 and STA-955), the TiB reinforcement layer's morphology and the strengthening effect on the composites can be attributed to the trend of the TiB reinforcement layer from a quasi-continuous to a continuous layer.

The mechanical properties of TiB-reinforced TMCs are jointly determined by the Ti-6Al-4V matrix and TiB reinforcement [24,36,51,52]. TiBw reinforcement will effectively hinder the movement of dislocations, leading to the piling-up of dislocations, and improve the strength of the material. Boehlert et al. [53] have reported that because the modulus of TiB (450 GPa) is higher than that of Ti-6Al-4V matrix (113.8 GPa) and because of the good bonding interface between Ti-6Al-4V matrix and TiB reinforcement, the TiB will fracture first as the load increases. In addition, this phenomenon can also be observed in Figure 11a–c of this experiment. Therefore, due to the pile-up of dislocations, the stress concentration area delineated by the gray areas in Figure 13 will first form at the fracture position of the TiB whisker [54]. The fractured TiB will become the starting point of crack propagation. When the crack propagates through the Ti-6Al-4V area, the matrix phase will release the high stress at the crack tip to prevent the crack from propagating [55]. However, the large agglomeration of TiB whiskers and the broadening of reinforcement layers (Figure 7a–d) lead to the weakening of the enhancement effect of the matrix phase (Figure 11c,d), and the cracks will rapidly expand and coalesce, resulting in a decrease in the properties of the composite material. When the addition of boron powder is less than 3 vol.% (Figure 7a,b), some dislocations accumulate and entangle in the matrix phase/TiB interface, and some pile up at the grain boundaries (Figure 13a,b). As the stress increases, dislocations at the matrix phase/TiB interface cause stress concentration, resulting in fracture of the reinforcement phases, whereas dislocations at the grain boundaries cause material yield by passing through the grain boundaries. When more than 5 vol.% boron powder is added, TiB covers the majority of the grain boundaries (Figure 7c,d). Due to the good bonding interface between with Ti-6Al-4V matrix and TiB reinforcement, the dislocation could not cross the TiB boundary, resulting in a large number of dislocations accumulating at the interface of the matrix phase/TiB (Figure 13c). Severe stress concentration led to a large number of TiB fractures; the cracks rapidly expanded, and the material yield disappeared.

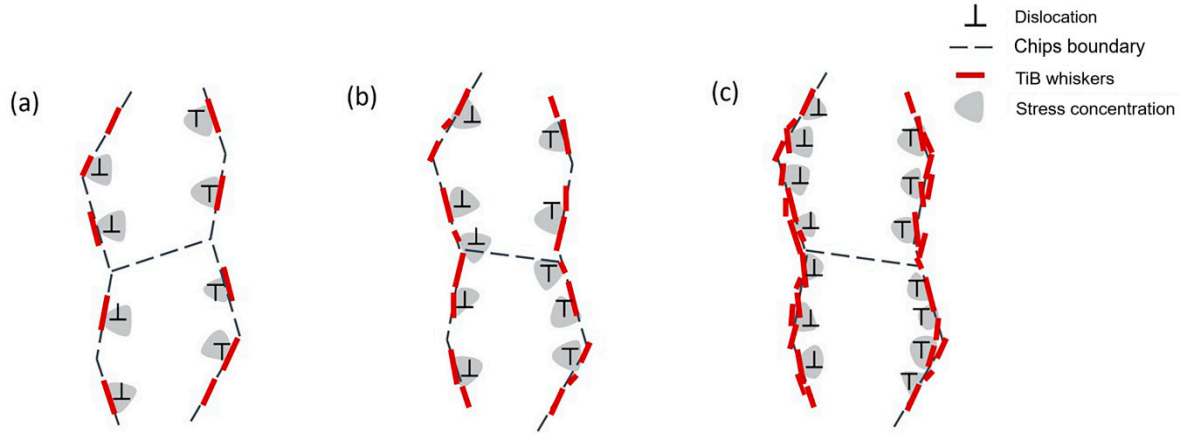


**Figure 13.** Schematic illustrations of dislocation mechanisms in (**a**) discontinuous TiB reinforcement layers; (**b**) quasi-continuous TiB reinforcement layers; and (**c**) continuous TiB reinforcement layers.

It is worth noting that when the addition of boron reaches 5 vol.%, the material's yield disappears and the composite material exhibits brittle fracture, which is inconsistent with the experimental results observed by most scholars [37,48,56,57]. This is because, in multi-phase alloys, the mechanical properties are mainly affected by the stress distribution among the microstructural components [58]. In the published works, TiBw/Ti-6Al-4V composites are mostly fabricated with Ti64 pre-alloyed (or master alloy) powder and $TiB_2$ (or boron) powder [23,27,37,50]. Therefore, the distribution of TiB whiskers is relatively

uniform, and the TiB whiskers are mostly formed in a network (along the grain boundaries) or point shape [23,57]. Due to the uniform distribution of TiB whiskers, the stress distribution between the reinforcement phase and the matrix phase is more uniform during the tensile process, which makes TiBw tend to inhibit the movement of the matrix phase near each TiBw [57]. However, in the present work, due to the shape of the raw materials (Ti64 chips), the TiBw were formed at the prior chip boundaries, which made the TiBw exhibit a layered structure in the matrix phase, resulting in more severe aggregation and uneven stress distribution of the TiBw when the boron addition increased (5 vol.% and 7 vol.%). Furthermore, the continuously distributed and thickened TiB reinforcement layers divide the Ti64 matrix phases and TiB reinforcement phases into isolated regions, which significantly weakens the ability of the system to coordinate deformation; thus, the properties of the composites with a 5 vol.% boron addition are slightly different from the existing experimental results.

## 4. Conclusions

In the present study, low-cost and high-performance titanium alloy matrix composites (TiBw/Ti6Al4V composites) were successfully fabricated using Ti-6Al-4V machining chips and boron powder. Based on an investigation of their microstructures and mechanical properties, it was found that:

1. The microstructural feature of the TiB structure experiences the variation of discontinuous TiB reinforcement layers (Chips-Ti64-1TiB) → quasi-continuous TiB reinforcement layers (Chips-Ti64-3TiB) → continuous TiB reinforcement layers (Chips-Ti64-5TiB and Chips-Ti64-7TiB) with the increased boron addition;
2. With the increase of the amount of boron addition (1 vol.%, 3 vol.%, 5 vol.%, and 7 vol.%), both UTS and YS of the fabricated composites hot-pressed at 1250°C were first increased and then decreased; the composites with 1 vol.% and 3 vol.% boron addition show optimized mechanical properties, having a UTS of 1085 MPa and 1127 MPa, respectively, and a strain of failure of 5.83% and 3.98%, respectively;
3. After heat treatments STA-855 and STA-955, the strength of the Chips-Ti64-3TiB increases to UTS of 1184 MPa, YS of 1083 MPa, and UTS of 1231 MPa, YS of 1139 MPa, respectively, but the ductility decreases sharply due to the coarsening of TiB whiskers.

**Author Contributions:** Conceptualization, F.Y.; methodology, F.Y., L.B., Y.Q. and Y.L.; software, Y.Z.; validation, F.Y., L.B., Y.Q. and Y.L.; formal analysis, Y.Z.; investigation, F.Y. and Y.Z.; resources, F.Y.; data curation, F.Y. and Y.Z.; writing—original draft preparation, Y.Z.; writing—review and editing, F.Y. and A.P.S.; visualization, Y.Z.; supervision, F.Y.; project administration, F.Y. All authors have read and agreed to the published version of the manuscript.

**Funding:** This research received no external funding.

**Institutional Review Board Statement:** Not applicable.

**Informed Consent Statement:** Not applicable.

**Data Availability Statement:** The data presented in this study are available upon request from the corresponding author.

**Acknowledgments:** The authors gratefully acknowledge Ma Qian from RMIT University for providing Ti-6Al-4V chip materials.

**Conflicts of Interest:** The authors declare no conflict of interest.

## References

1. Tjong, S.C.; Mai, Y.M. Processing-structure-property aspects of particulate and whisker reinforced titanium matrix composites. *Compos. Sci. Technol.* **2008**, *68*, 583–601. [CrossRef]
2. Morsi, K.; Patel, V.V. Processing and properties of titanium-titanium boride (TiBw) matrix composites-a review. *J. Mater. Sci.* **2007**, *42*, 2037–2047. [CrossRef]

3. Shalnova, S.A.; Volosevich, D.V.; Sannikov, M.I.; Magidov, I.S.; Mikhaylovskiy, K.V.; Turichin, G.A.; Klimova-Korsmik, O.G. Direct energy deposition of SiC reinforced Ti–6Al–4V metal matrix composites: Structure and mechanical properties. *Ceram. Int.* **2022**, *48*, 35076–35084.
4. Lagos, M.A.; Agote, I.; Atxaga, G.; Adarraga, O.; Pambaguian, L. Fabrication and characterisation of Titanium Matrix Composites obtained using a combination of Self propagating High temperature Synthesis and Spark Plasma Sintering. *Mater. Sci. Eng. A* **2016**, *655*, 44–49. [CrossRef]
5. Singh, G.; Sharma, N.; Kumar, D.; Hegab, H. Design, development and tribological characterization of Ti–6Al–4V/hydroxyapatite composite for bio-implant applications. *Mater. Chem. Phys.* **2020**, *243*, 122662. [CrossRef]
6. Jenczyk, P.; Grzywacz, H.; Milczarek, M.; Jarząbek, D.M. Mechanical and Tribological Properties of Co-Electrodeposited Particulate-Reinforced Metal Matrix Composites: A Critical Review with Interfacial Aspects. *Materials* **2021**, *14*, 3181. [CrossRef]
7. Dariusz Jarząbek, M. The impact of weak interfacial bonding strength on mechanical properties of metal matrix—Ceramic reinforced composites. *Compos. Struct.* **2018**, *201*, 352–362. [CrossRef]
8. Hayat, M.D.; Singh, H.; He, Z.; Cao, P. Titanium metal matrix composites: An overview. *Compos. Part A Appl. Sci. Manuf.* **2019**, *121*, 418–438. [CrossRef]
9. Lu, W.; Zhang, D.; Zhang, X.; Wu, R.; Sakata, T.; Mori, H. Microstructural characterization of TiB in in situ synthesized titanium matrix composites prepared by common casting technique. *J. Alloys Compd.* **2001**, *327*, 240–247. [CrossRef]
10. Singh, N.; Hameed, P.; Ummethala, R.; Manivasagam, G.; Prashanth, K.G.; Eckert, J. Selective laser manufacturing of Ti-based alloys and composites: Impact of process parameters, application trends, and future prospects. *Mater. Today* **2020**, *8*, 100097. [CrossRef]
11. Murr, L.E.; Quinones, S.A.; Gaytan, S.M.; Lopez, M.I.; Rodela, A.; Martinez, E.Y.; Hernandez, D.H.; Martinez, E.; Medina, F.; Wicker, R.B. Microstructure and mechanical behavior of Ti-6Al-4V produced by rapid-layer manufacturing, for biomedical applications. *J. Mech. Behav. Biomed. Mater.* **2009**, *2*, 20–32. [CrossRef]
12. Lui, E.W.; Palanisamy, S.; Dargusch, M.S.; Xia, K. Effects of chip conditions on the solid state recycling of Ti-6Al-4V machining chips. *J. Mater. Process* **2016**, *238*, 297–304. [CrossRef]
13. Luo, P.; McDonald, D.T.; Palanisamy, S.; Dargusch, M.S.; Xia, K. Ultrafine-grained pure Ti recycled by equal channel angular pressing with high strength and good ductility. *J. Mater. Process* **2013**, *213*, 469–476. [CrossRef]
14. Zhao, Q.Y.; Pi, Z.; Lu, X.; Qu, Y.; Bolzoni, L.; Yang, F. Superior strength-ductility balance in hot pressed swarf-Ti-6Al–4V alloy. *Mater. Sci. Eng. A* **2020**, *788*, 139574. [CrossRef]
15. Gao, L.; Li, X.-M.; Huang, H.-G.; Sui, Y.-D.; Zhang, H.-M.; Shi, Z.; Chattopadhyay, K.; Jiang, Y.-H.; Zhou, R. Numerical study of aluminum segregation during electron beam cold hearth remelting for large-scale Ti-6 wt%Al-4 wt%V alloy round ingot. *Int. J. Heat Mass Transf.* **2019**, *139*, 764–772. [CrossRef]
16. Delzant, P.O.; Chapelle, P.; Jardy, A.; Jourdan, J.; Jourdan, J.; Millet, Y. Investigation of arc dynamics during vacuum arc remelting of a Ti64 alloy using a photodiode based instrumentation. *J. Mater. Process. Technol.* **2019**, *266*, 10–18. [CrossRef]
17. Moon, B.M.; Seo, J.H.; H.-Lee, J.; Jung, K.H.; Park, J.H.; H.-Jung, D. Method of recycling titanium scraps via the electromagnetic cold crucible technique coupled with calcium treatment. *J. Alloys Compd.* **2017**, *727*, 931–939. [CrossRef]
18. Shamsudin, S.; Lajis, M.A.; Zhong, Z.W. Evolutionary in Solid State Recycling Techniques of Aluminium: A review. *Procedia CIRP* **2016**, *40*, 256–261. [CrossRef]
19. Yang, F.; Pi, Z.Q.; Zhao, Q.Y.; Raynova, S.; Liu, Q.; Sharp, K.; Brandt, M.; Bolzoni, L.; Qian, M. Strong and Ductile Ti-6Al-4V Alloy Produced by Hot Pressing of Ti-6Al-4V Swarf. *JOM* **2019**, *71*, 1056–1061. [CrossRef]
20. Topolski, K.; Bochniak, W.; Łagoda, M.; Ostachowski, P.; Garbacz, H. Structure and properties of titanium produced by a new method of chip recycling. *J. Mater. Process. Technol.* **2017**, *248*, 80–91. [CrossRef]
21. Topolski, K.; Ostachowski, P. Solid state processing of titanium chips by an unconventional plastic working. *J. Mater. Res. Technol.* **2021**, *13*, 808–822. [CrossRef]
22. Luo, P.; McDonald, D.T.; Zhu, S.M.; Palanisamy, S.; Dargusch, M.S.; Xia, K. Analysis of microstructure and strengthening in pure titanium recycled from machining chips by equal channel angular pressing using electron backscatter diffraction. *Mater. Sci. Eng. A* **2012**, *538*, 252–258. [CrossRef]
23. Lu, H.; Zhang, D.; Gabbitas, B.; Yang, F.; Matthews, S. Synthesis of a TiBw/Ti6Al4V composite by powder compact extrusion using a blended powder mixture. *J. Alloys Compd.* **2014**, *606*, 262–268. [CrossRef]
24. Xinghong, Z.; Qiang, X.; Jiecai, H.; Kvanin, V.L. Self-propagating high temperature combustion synthesis of TiB/Ti composites. *Mater. Sci. Eng. A* **2003**, *348*, 41–46. [CrossRef]
25. Tao, X.; Yao, Z.; Zhang, S. Reconstruction and refinement of TiB whiskers in titanium matrix composite after electron beam remelting. *Mater. Lett.* **2018**, *225*, 13–16. [CrossRef]
26. Sen, I.; Tamirisakandala, S.; Miracle, D.B.; Ramamurty, U. Microstructural effects on the mechanical behavior of B-modified Ti-6Al-4V alloys. *Acta Mater.* **2007**, *55*, 4983–4993. [CrossRef]
27. An, Q.; Huang, L.; Jiang, S.; Bao, Y.; Ji, M.; Zhang, R.; Geng, L. Two-scale TiB/Ti64 composite coating fabricated by two-step process. *J. Alloys Compd.* **2018**, *755*, 29–40. [CrossRef]
28. Pinke, P.; Čaplovič, L.; Kovács, T. The Influence of Heat Treatment on the Microstructure of the Casted Ti6Al4V Titanium Alloy. Slovak University of Technology Bratislava, 2011, web, 11. Available online: https://www.kfki.hu/anyagokvilaga/tartalom/2007/oktober/Pinke_2.pdf (accessed on 24 October 2022).

29. Yang, F.; Ajit, S.R.; Singh, Q.; Zhao, Y.; Villarreal, C.R.; Bolzoni, L. Producing High-Quality Titanium Alloy by a Cost-Effective Route Combining Fast Heating and Hot Processing. *JOM* **2018**, *70*, 632–637. [CrossRef]
30. Yang, F.; Gabbitas, B. Feasibility of producing Ti-6Al-4V alloy for engineering application by powder compact extrusion of blended elemental powder mixtures. *J. Alloys Compd.* **2017**, *695*, 1455–1461. [CrossRef]
31. Gammon, L.M.; Briggs, R.D.; Packard, J.M.; Batson, K.W.; Boyer, R.; Domby, C.W. Metallography and microstructures of titanium and its alloys. *ASM Handb.* **2004**, *9*, 899–917.
32. Zhang, X.H.; Qu, W.; He, X.D.; Kvanin, V.L. Self-propagating high temperature combustion synthesis of TiC/$TiB_2$ ceramic-matrix composites. *Compos. Sci. Technol.* **2002**, *62*, 2037–2041.
33. Guo, Y.; Genelot, P.; Singh, A.P.; Bolzoni, L.; Qu, Y.; Kou, H.; Lin, J.; Yang, F. High-Strength Near-Beta Titanium Alloy Fabricated by Direct Hot Pressing of the Machining Swarf. *J. Mater. Eng. Perform.* **2022**, *31*, 8619–8629. [CrossRef]
34. Koo, M.Y.; Park, J.S.; Park, M.K.; Kim, K.T.; Hong, S.H. Effect of aspect ratios of in situ formed TiB whiskers on the mechanical properties of TiBw/Ti–6Al–4V composites. *Scr. Mater.* **2012**, *66*, 487–490. [CrossRef]
35. Godfrey, T.; Wisbey, A.; Goodwin, P.; Bagnall, K.; Ward-Close, C. Microstructure and tensile properties of mechanically alloyed Ti–6A1–4V with boron additions. *Mater. Sci. Eng. A* **2000**, *282*, 240–250. [CrossRef]
36. Soboyejo, W.O.; Shen, W.; Srivatsan, T.S. An investigation of fatigue crack nucleation and growth in a Ti–6Al–4V/TiB in situ composite. *Mech. Mater.* **2004**, *36*, 141–159. [CrossRef]
37. Zhang, R.; Huang, L.; Zhao, X.; Geng, L.; Wang, S.; Jiang, S.; Jiao, Y. Influence of deformation parameters and network structure to the microstructure evolution and flow stress of TiBw/Ti64 composite. *Mater. Sci. Eng. A* **2021**, *809*, 140997. [CrossRef]
38. Abbas, A.; Seif, A.; El-Mahallawi, I.; Khalifa, W. Microstructure and Hardness of Subzero Quenched and Heat Treated Ti-6Al-4V Alloy. *TMS* **2017**, *379*, 379–391.
39. Zhang, Z.; Qin, J.; Zhang, Z.; Chen, Y.; Lu, W.; Zhang, D. Effect of β heat treatment temperature on microstructure and mechanical properties of in situ titanium matrix composites. *Mater. Des.* **2010**, *31*, 4269–4273. [CrossRef]
40. Wang, B.; Huang, L.J.; Geng, L. Effects of heat treatments on the microstructure and mechanical properties of as-extruded TiBw/Ti6Al4V composites. *Mater. Sci. Eng. A* **2012**, *558*, 663–667. [CrossRef]
41. Li, H.; Jia, D.; Yang, Z.; Liao, X.; Jin, H.; Cai, D.; Zhou, Y. Effect of heat treatment on microstructure evolution and mechanical properties of selective laser melted Ti–6Al–4V and TiB/Ti–6Al–4V composite: A comparative study. *Mater. Sci. Eng. A* **2021**, *80*, 140415. [CrossRef]
42. Feng, H.B.; Zhou, Y.; Jia, D.C.; Meng, Q.C.; Rao, J.C. Growth Mechanism of In Situ TiB Whiskers in Spark Plasma Sintered TiB/Ti Metal Matrix Composites. *Cryst. Growth Des.* **2006**, *6*, 1626–1630. [CrossRef]
43. Verma, S.; Kumar, S.; Gokhale, R.; Burgess, D.J. Physical stability of nanosuspensions: Investigation of the role of stabilizers on Ostwald ripening. *Int. J. Pharm.* **2011**, *406*, 145–152. [CrossRef] [PubMed]
44. Zhang, J.; Song, B.; Cai, C.; Zhang, L.; Shi, Y. Tailorable microstructure and mechanical properties of selective laser melted TiB/Ti–6Al–4V composite by heat treatment. *Adv. Powder Mater.* **2022**, *1*, 100010. [CrossRef]
45. Gorsse, S.; Miracle, D.B. Mechanical properties of Ti-6Al-4V/TiB composites with randomly oriented and aligned TiB reinforcements. *Acta Mater.* **2003**, *51*, 2427–2442. [CrossRef]
46. Qin, D.; Li, Y.; Zhang, S.; Zhou, L. On the tensile embrittlement of lamellar Ti–5Al–5V–5Mo–3Cr alloy. *J. Alloys Compd.* **2016**, *663*, 581–593. [CrossRef]
47. Huang, L.J.; Geng, L.; Peng, H.X. In situ (TiBw+TiCp)/Ti6Al4V composites with a network reinforcement distribution. *Mater. Sci. Eng. A.* **2010**, *527*, 6723–6727. [CrossRef]
48. Huang, L.J.; Geng, L.; Wang, B.; Xu, H.Y.; Kaveendran, B. Effects of extrusion and heat treatment on the microstructure and tensile properties of in situ TiBw/Ti6Al4V composite with a network architecture. *Compos. Part. A. Appl. Sci.* **2012**, *43*, 486–491. [CrossRef]
49. Qi, Y.; Timokhina, I.B.; Shekhter, A.; Sharp, K.; Lapovok, R. Optimization of upcycling of Ti-6Al-4V swarf. *J. Mater. Process. Technol.* **2018**, *255*, 853–864. [CrossRef]
50. Jia, M.; Alshammari, Y.; Yang, F.; Bolzoni, L. Mechanical behaviour of flashless hot forged and heat treated TiB-reinforced Ti–6Al–4V composites. *Mater. Chem. Phys.* **2022**, *290*, 12662. [CrossRef]
51. Cai, C.; He, S.; Li, L.; Teng, Q.; Song, B.; Yan, C.; Wei, Q.; Shi, Y. In-situ TiB/Ti-6Al-4V composites with a tailored architecture produced by hot isostatic pressing: Microstructure evolution, enhanced tensile properties and strengthening mechanisms. *Compos. Eng. B.* **2019**, *164*, 546–558. [CrossRef]
52. Dong, Y.P.; Li, Y.L.; Zhou, S.Y.; Zhou, Y.H.; Dargusch, M.S.; Peng, H.X.; Yan, M. Cost-affordable Ti-6Al-4V for additive manufacturing: Powder modification, compositional modulation and laser in-situ alloying. *Addit. Manuf.* **2021**, *37*, 101699. [CrossRef]
53. Boehlert, C.J.; Cowen, C.J.; Tamirisakandala, S.; McEldowney, D.J.; Miracle, D.B. In situ scanning electron microscopy observations of tensile deformation in a boron-modified Ti–6Al–4V alloy. *Scr. Mater.* **2006**, *55*, 465–468. [CrossRef]
54. Du, Z.X.; Xiao, S.L.; Wang, P.X.; Xu, L.J.; Chen, Y.Y.H.; Rahoma, K.S. Effects of trace TiB and TiC on microstructure and tensile properties of β titanium alloy. *Mater. Sci. Eng. A* **2014**, *596*, 71–79. [CrossRef]
55. Zhang, W.; Wang, M.; Chen, W.; Feng, Y.; Yu, Y. Preparation of TiBw/Ti–6Al–4V composite with an inhomogeneous reinforced structure by a canned hot extrusion process. *J. Alloys Compd.* **2016**, *669*, 79–90. [CrossRef]
56. Zhou, Z.G.; Liu, Y.Z.; Liu, X.H. Constructing targeted bi-lamellar microstructure via heat treatment for high compressive strength and plasticity in selective laser melted Ti6Al4V-5vol%TiB composite. *Mater. Sci. Eng. A* **2022**, *884*, 143173. [CrossRef]

57. Zhou, Z.G.; Liu, Y.Z.; Liu, X.H.; Zhan, Q.K.; Wang, K.D. Microstructure evolution and mechanical properties of in-situ Ti6Al4V–TiB composites manufactured by selective laser melting. *Compos. Eng. B.* **2021**, *207*, 108567. [CrossRef]
58. Lei, L.; Zhao, Q.Y.; Wu, C.; Zhao, Y.Q.; Huang, S.X.; Jia, W.J.; Zeng, W.D. Variant selection, coarsening behavior of α phase and associated tensile properties in an α+β titanium alloy. *J. Mater. Sci. Technol.* **2022**, *99*, 101–113. [CrossRef]